THE JOURNAL OF BIOLOGICAL CHEMISTRY VOL. 281, NO. 3, pp. 1817–1826, January 20, 2006
Printed in the U.S.A.

Staphylococcus aureus Sortase A Transpeptidase

CALCIUM PROMOTES SORTING SIGNAL BINDING BY ALTERING THE MOBILITY AND STRUCTURE OF AN ACTIVE SITE LOOP*[S]

Received for publication, June 6, 2005, and in revised form, October 17, 2005 Published, JBC Papers in Press, November 3, 2005, DOI 10.1074/jbc.M506123200

Mandar T. Naik[‡§], Nuttee Suree[‡§], Udayar Ilangovan[‡§], Chu Kong Liew[‡§], William Thieu[‡§], Dean O. Campbell[‡§], Jeremy J. Clemens[‡], Michael E. Jung[‡], and Robert T. Clubb[‡¶1]

From the [‡]Department of Chemistry & Biochemistry, [§]UCLA-Department of Energy Institute for Genomics and Proteomics, and [¶]Molecular Biology Institute, University of California, Los Angeles, California 90095-1570

Many virulence factors in Gram-positive bacteria are covalently anchored to the cell-wall peptidoglycan by sortase enzymes, a group of widely distributed cysteine transpeptidases. The *Staphylococcus aureus* Sortase A protein (SrtA) is the archetypal member of the Sortase family and is activated by Ca^{2+}, an adaptation that may facilitate host colonization as elevated concentrations of this ion are encountered in human tissue. Here we show that a single Ca^{2+} ion bound to an ordered pocket on SrtA allosterically activates catalysis by modulating both the structure and dynamics of a large active site loop. Detailed nitrogen-15 relaxation measurements indicate that Ca^{2+} may facilitate the adaptive recognition of the substrate by inducing slow micro- to millisecond time-scale dynamics in the active site. Interestingly, relaxation compensated Carr-Purcell-Meiboom-Gill experiments suggest that the time scale of these motions is directly correlated with ion binding. The results of site-directed mutagenesis indicate that this motional coupling is mediated by the side chain of Glu-171, which is positioned within the $\beta6/\beta7$ loop and shown to contribute to Ca^{2+} binding. The available structural and dynamics data are compatible with a loop closure model of Ca^{2+} activation, in which the $\beta6/\beta7$ loop fluctuates between a binding competent closed form that is stabilized by Ca^{2+}, and an open, highly flexible state that removes key substrate contacting residues from the active site.

Surface proteins on bacteria are frequently virulence factors, promoting bacterial adhesion, resistance to phagocytic killing, and host cell invasion during infection. In Gram-positive bacteria these proteins are often covalently anchored to the cell wall by sortase enzymes, a family of novel cysteine transpeptidases (1–3). The sortase A protein (SrtA)[2] from *Staphylococcus aureus* has been characterized extensively (4) and anchors proteins bearing a cell wall sorting signal that consists of a conserved LP*X*TG motif (where *X* is any amino acid), a hydrophobic domain, and a tail of mostly positively charged residues (4–6). SrtA cleaves in between the threonine and glycine of the LP*X*TG motif (7) and catalyzes the formation of a peptide bond between the carboxyl-group of the threonine and the amine-group of the cell-wall precursor lipid II (7–9). The lipid II-linked protein is then incorporated into the peptidoglycan of the cell wall via the transglycosylation and transpeptidation reactions of bacterial cell-wall synthesis. Sortases represent an attractive target for new anti-infective agents, because they are widely distributed among a variety of bacterial pathogens (10, 11) (*e.g. Bacillus anthracis*, *Listeria monocytogenes*, *Streptococcus pneumoniae*, and *Streptococcus pyogenes*), and have been shown to be required for virulence (12–16).

The catalytic domain of SrtA ($SrtA_{\Delta N59}$, residues 60–206) adopts a conserved eight-stranded β-barrel fold (17, 18). The active site is organized around the catalytically essential side chain of Cys-184, whose thiolate nucleophilically attacks the threonine carbonyl carbon within the LP*X*TG sorting signal, forming a thioester linkage between the enzyme and substrate (19). In addition to Cys-184, the hydrophilic side chains of His-120 and Arg-197 are absolutely required for catalysis (20–22). These residues likely participate in general acid/base catalysis, and one of them must activate the thiol for nucleophilic attack, because it is protonated at neutral pH (23). The indole ring of Trp-194 partially shields the cysteine thiol from the solvent, and its mutation to alanine reduces enzyme activity 4-fold through an unknown mechanism (20). Using NMR and crystallography, the LP*X*TG sorting signal binding site has recently been localized to a surface formed by strands $\beta4$ and $\beta7$, and to a proximal loop that connects strands $\beta6$ to $\beta7$(the $\beta6/\beta7$ loop) (18, 22). Substrate binding may occur through an induced-fit mechanism involving conformational changes in the $\beta6/\beta7$ loop, because it is disordered in the absence of the sorting signal substrate (17, 18).

Ca^{2+} stimulates the activity of $SrtA_{\Delta N59}$ *in vitro* (17) and may enable *S. aureus* to increase the rate of surface protein anchoring as it encounters elevated concentrations of this ion at sites of infection. Because many surface proteins function as virulence factors, the stimulatory effect of Ca^{2+} likely plays an important role in the infection process. Previously we showed that Ca^{2+} bound to an ordered pocket positioned distal to the active site (hereafter referred to as the $\beta3/\beta4$ pocket) (17). However, this work did not reveal how Ca^{2+} stimulated enzyme activity. Here we show using enzyme kinetic and detailed NMR nitrogen-15 measurements that a single Ca^{2+} ion bound to the $\beta3/\beta4$ pocket promotes substrate binding. We provide evidence that ion binding to this distal site allosterically controls enzyme activity by altering motions in the active site $\beta6/\beta7$ loop. In particular, we show that Ca^{2+} retards motions and induces slow micro- to millisecond time-scale dynamics within the loop that may promote the adaptive recognition of the substrate. The results of relaxation compensated Carr-Purcell-Meiboom-Gill (CPMG) experiments suggest that the active site motions are correlated with the rate of ion binding. The results of site-directed mutagenesis suggest that this motional coupling is mediated by the side chain of Glu-171, which is located at the C-terminal end of the $\beta6/\beta7$ loop and required for high affinity ion binding. This work represents the

* This work was supported by National Institutes of Health Grant AI52217 (to R. T. C. and M. E. J.). The costs of publication of this article were defrayed in part by the payment of page charges. This article must therefore be hereby marked "*advertisement*" in accordance with 18 U.S.C. Section 1734 solely to indicate this fact.

[S] The on-line version of this article (available at http://www.jbc.org) contains supplemental Fig. S1 and Tables S1–S3.

[1] To whom correspondence should be addressed: Dept. of Chemistry & Biochemistry, University of California, Los Angeles, 405 Hilgard Ave., Los Angeles, CA 90095-1570. Tel.: 310-206-2334; Fax: 310-206-4749; E-mail: rclubb@mbi.ucla.edu.

[2] The abbreviations used are: SrtA, sortase A protein; CPMG, Carr-Purcell-Meiboom-Gill; rc-CPMG, relaxation-compensated CPMG; NOE, nuclear Overhauser effect; HSQC, heteronuclear single quantum coherence.

first NMR dynamics study of a sortase enzyme and reveals that complex conformational dynamics contribute to the function of these enzymes.

MATERIALS AND METHODS

Protein Preparation and Purification—Uniformly ^{15}N-enriched $SrtA_{\Delta N59}$ (residues 60–206) was obtained as previously described (17). Three separate samples of 3 mM ^{15}N $SrtA_{\Delta N59}$ were prepared for relaxation studies by dissolving weighed lyophilized protein in 500 μl of 50 mM Tris-HCl, 100 mM NaCl, 3 mM dithiothreitol, 7% D_2O, and 0.01% NaN_3. The pH of the sample was adjusted to 6.20 (uncorrected for the deuterium effect). Each sample differed in the amount of Ca^{2+} present: 1) no Ca^{2+} (apo-Ca^{2+} $SrtA_{\Delta N59}$), 2) 20 μM of $CaCl_2$, or 3) 20 mM Ca^{2+} (Ca^{2+}-bound $SrtA_{\Delta N59}$). Where needed, the water used for the samples was preconditioned with Chelex resin. The Mn^{2+} and Ca^{2+} titration experiments were conducted on similar samples of ^{15}N $SrtA_{\Delta N59}$ using defined amounts of these ions. The histidine-tagged single amino acid mutants of sortase were purified using a nickel column and exchanged into the appropriate buffer for enzymatic and NMR studies.

Modification of $SrtA_{\Delta N59}$ by the Peptidyl-Sulfhydryl Compound—A peptidyl-sulfhydryl compound (benzoyloxycarbonyl-Leu-Pro-Ala-Thr with a C-terminal -CH_2SH group) was used to modify $SrtA_{\Delta N59}$ (the synthesis of the compound will be reported elsewhere). A 5-fold molar excess of the compound was added to two samples of $SrtA_{\Delta N59}$ (500 μl of a 20 μM protein solution) in buffer I (pH 8.0, 50 mM Tris-HCl, and 100 mM NaCl), one without Ca^{2+} and one containing 20 mM $CaCl_2$. The mixture was incubated on a rotating wheel at room temperature, and samples were removed periodically and analyzed using reverse phase high-performance liquid chromatography on a C18 column (Waters, Mildford, MA). The areas under the peaks corresponding to modified and unmodified SrtA in the chromatogram were integrated to calculate the percentage of modification at each time point.

Site-directed Mutagenesis—Wild-type $SrtA_{\Delta N59}$ plasmid containing a C-terminal 6-His tag was generated as described previously (24). Single amino acid mutations of $SrtA_{\Delta N59}$ were generated by PCR using the $SrtA_{\Delta N59}$ plasmid template and *Pfu* Turbo DNA polymerase (Stratagene). The Glu-108 codon was mutated to encode Ala-108 using the primers E108A-F (TAAGCTTTGCAGAAGAAAATGCATCACTAGATGATCAAAATATTT) and E108A-R (AAATATTTTGATCATCTAGTGATGCATTTTCTTCTGCAAAGCTTA). The Asp-170 codon was mutated to encode Ala-170 using the primers D170A-F (ACAGATGTAGGAGTTCTAGCAGAACAAAAAGGTAAAGATAA) and D170A-R (TTATCTTTACCTTTTTGTTCTGCTAGAACTCCTACATCTGT). The Glu-171 codon was mutated to encode Ala-171 using the primers E171A-F (CAGATGTAGGAGTTCTAGATGCACAAAAAGGTAAAGATAAACAATT) and E171A-R (AATTGTTTATCTTTACCTTTTTGTGCATCTAGAACTCCTACATCTG) (underlined nucleotides mark mutational changes). The identity of the mutants was confirmed by DNA sequencing. Purification of the wild-type and mutant enzymes was performed as previously described (24).

Enzyme Kinetics Measurements—A self-quenched fluorescent peptide, *o*-aminobenzoyl-LPETG-2,4-dinitrophenyl, was used as a substrate in the cleavage reaction as previously described (25). Reactions contained 1.5 μM $SrtA_{\Delta N59}$ enzyme in the assay buffer (20 mM HEPES, pH 7.5, with various concentrations of $CaCl_2$). The aminobenzoyl-LPETG-dinitrophenyl substrate was dissolved in Me_2SO and added to the reaction to a final concentration between 6.25 and 25 μM, for a total reaction volume of 200 μl. The increase in fluorescence intensity was monitored at room temperature using excitation at 335 nm and recording the emission maximum at 420 nm on a SPEX spectrofluorometer (Photon Technology International, Lawrenceville, NJ). The steady-state velocities (V_s) from the biphasic progress curves were calculated as described previously (25). The progress curves were fit to the following equation,

$$P = \pi[1 - \exp(-k_{obs}t) + V_s t] \qquad \text{(Eq. 1)}$$

where π is the amplitude of the burst phase. The kinetic parameters were calculated from the substrate dependence of V_s as described previously (25).

Relaxation Data Acquisition and Processing—NMR data were acquired on Bruker Avance 500- and 600-MHz spectrometers equipped with 5-mm triple resonance cryo-probes and single axis pulsed field gradients. The chemical shift assignments have been reported previously for SrtA in the presence of 20 mM $CaCl_2$ (17) (BioMagResBank Code 4879), and near complete backbone assignments for the apo-Ca^{2+} form of the protein were obtained using standard triple resonance techniques.[3] The ^{15}N spin-lattice/longitudinal (R_1), and spin-spin/transverse (R_2) relaxation rates, and the steady-state heteronuclear {^{1}H}-^{15}N NOE values were measured as previously described (26–28). Ten R_1 two-dimensional experiments were performed in random order, with relaxation delays of 42 (duplicate), 167, 335, 544 (duplicate), 816, 1172, 1591, and 2428 ms. Similarly, R_2 experiments were performed randomly with relaxation delays of 17 (duplicate), 35, 52 (duplicate), 69, 86, 104, 121, and 138 ms. The NOE experiment was carried out in an interleaved manner, with and without proton saturation and repeated thrice under identical conditions. All experiments were acquired with 2048 × 256 complex points in the F2 and F1 dimensions with corresponding spectral widths of 10,000 and 2,027 Hz, and the proton carrier frequency was set to the water resonance. The data sets were processed using nmrPipe (29), and peak heights were determined using Sparky (30) operating on a Linux work station.

The following programs used to analyze the relaxation data were kindly provided by Prof. Arthur G. Palmer 3rd at Columbia University: Curvefit, Pbdinertia, R2R1_Diffusion, Quadric Diffusion, and Modelfree 4.01. The rate constants were evaluated using the program Curvefit, assuming mono-exponential decay of the peak intensities. The errors in peak intensities were calculated from the two duplicate experiments using a Perl language script kindly provided by Prof. Patrick Loria at Yale University. The error in the Heteronuclear NOEs was calculated by propagating the base-plane noise as calculated from the signal-to-noise ratio and is the average derived from three experiments. The ^{1}H-^{15}N HSQC spectra of $SrtA_{\Delta N59}$ in both the absence and presence of Ca^{2+} are well resolved, enabling the reliable measurement of relaxation parameters for 92 and 98 residues respectively, out of a total of 148. The average R_1, R_2, and {^{1}H}-^{15}N NOE parameters for apo-Ca^{2+} $SrtA_{\Delta N59}$ are, respectively, 1.59 ± 0.08 s^{-1}, 13.95 ± 5.80 s^{-1}, and 0.72 ± 0.29 at 500 MHz and 1.29 ± 0.08 s^{-1}, 14.84 ± 5.72 s^{-1}, and 0.77 ± 0.25 at 600 MHz. For Ca^{2+}-bound $SrtA_{\Delta N59}$, the average values are, respectively, 1.62 ± 0.10 s^{-1}, 13.38 ± 5.68 s^{-1}, and 0.80 ± 0.19 at 500 MHz and 1.30 ± 0.06 s^{-1}, 15.10 ± 8.71 s^{-1}, and 0.83 ± 0.16 at 600 MHz.

Optimization of Diffusion Tensor—Multiple approaches were used to assess the overall motion of $SrtA_{\Delta N59}$, because motional anisotropy also contributes to the R_2 values, and if miss-identified can cause erroneous internal correlation times (τ_e) and R_{ex} values (31, 32). The principal moments of the inertia tensor were calculated using the program Pdbinertia, and the values are 1.00:0.90:0.80 and 1.00:0.90:0.78, for the NMR solution structure of Ca^{2+}-bound $SrtA_{\Delta N59}$ (PDB accession code: 1IJA) and the Ca^{2+}-free crystal structure (PDB accession code: 1T2P) after the

[3] M. T. Naik, N. Suree, U. Ilangovan, C. K. Liew, W. Thieu, D. O. Campbell, J. J. Clemens, M. E. Jung, and R. T. Clubb, unpublished observation.

addition of hydrogen atoms using the program MolMol (33), respectively. Similar moments were obtained using the program HydroNMR version 5a (34), where the proteins were assumed to be hydrated with a 3.1 Å water shell (1.00:0.88:0.84 for Ca^{2+}-bound $SrtA_{\Delta N59}$ and 1.00:0.88:0.86 for apo-Ca^{2+} $SrtA_{\Delta N59}$). The latter analysis also provided an estimate of the molecular correlation time (τ_m) of each form of the protein: 11.03 and 9.89 ns for apo-Ca^{2+} and Ca^{2+}-bound $SrtA_{\Delta N59}$, respectively. Because the relative moments for both apo-Ca^{2+} and Ca^{2+}-bound $SrtA_{\Delta N59}$ vary significantly from a perfect sphere, the approach outlined by Tjandra *et al.* (31) was used to check the statistical significance of fitting the relaxation data to an axially symmetric model *versus* an isotropic model (R2R1_Diffusion program). These calculations were performed using data from residues whose R_2/R_1 ratios were within one standard deviation from the average R_2/R_1 ratio, and which had NOE ratios > 0.65 (35). The results from 500 MHz (and 600 MHz) data suggested a τ_m of 9.69 ns (9.54 ns) for Ca^{2+}-bound $SrtA_{\Delta N59}$ and a τ_m of 10.35 ns (9.94 ns) for apo-Ca^{2+} $SrtA_{\Delta N59}$. The data also showed a statistically significant improvement when using the axial symmetric model over the simple isotropic diffusion model. Interestingly, the Ca^{2+}-bound $SrtA_{\Delta N59}$ data fit best to a prolate ellipsoid, whereas the apo-Ca^{2+} $SrtA_{\Delta N59}$ data fit best assuming an oblate ellipsoid. This variation is mostly due to subtle differences in the $\beta6/\beta7$ loop orientation in the two structures. The tensor parameters were also calculated using the approach outlined by Bruschweiler *et al.* (36–38) using the program Quadric_Diffusion, which gave slightly elevated correlation times of 9.86 ns (9.80 ns) for Ca^{2+}-bound $SrtA_{\Delta N59}$ and 10.62 ns (10.17 ns) for apo-Ca^{2+} $SrtA_{\Delta N59}$ from 500 MHz (and 600 MHz) data, but the axial symmetric model was preferred over the isotropic or fully anisotropic models. The results from this final calculation were used as an initial guess for Modelfree analysis described below.

Modelfree Analysis—The amplitudes and effective correlation times for a protein's internal motions can be extracted from relaxation data using the Lipari-Szabo Modelfree formalism (39, 40). The analysis considers five semi-empirical forms of the spectral density function with each form composed of terms describing the motion of the N–H bond vector. This internal motion can be assumed to occur on two different, fast and slow time scales and can be characterized by effective correlation times, τ_f and τ_s (where $\tau_f \ll \tau_s \ll \tau_m$) and the square of order parameters, S_f^2 and S_s^2. The square of the generalized order parameters is defined as $S^2 = S_f^2 S_s^2$ and corresponds to the spatial restriction of the N–H bond vector (where $0 \leq S^2 \leq 1$). The analysis also accounts for line broadening due to chemical exchange, R_{ex}. All these motional parameters were fit to the spin-relaxation data using the program Modelfree 4.01 (41, 42). For each model, 500 randomly distributed data sets were generated, and model selection was done using a statistical testing protocol described by Mandel *et al.* (42). Initially, models were selected at fixed diffusion tensor parameters by comparing the sum-squared error of optimal fit with the 0.05 critical value of the distribution and wherever applicable, by *F*-test comparisons to the 0.20 critical value of the distribution. In the next step, after a model had been assigned to each spin, both the diffusion tensor and model parameters were optimized simultaneously. We used an N–H bond length of 1.02 Å and ^{15}N chemical shift anisotropy values of −160 ppm in our backbone spin calculations. For the sole tryptophan (Trp-136) side-chain spin, a chemical shift anisotropy value of −126 ppm was used (43). A minimum 3% base error is assumed in all parameters in the Modelfree analysis (44, 45). Out of 92 quantifiable residues in apo-Ca^{2+} $SrtA_{\Delta N59}$, 89 could be satisfactorily fit using Modelfree analysis (the relaxation data of Ser-70, Glu-95, and Ile-123 could not be fit). Model 1 (S^2-only) was an appropriate fit for 63 residues, 3 residues fit to model 2 (S^2 and τ_e), 13 residues fit to model 3 (S^2 and R_{ex}), 2 fit to model 4 (S^2, τ_e, and R_{ex}), and 11 residues fit to model 5 (S_f^2, S_s^2, and τ_e). In the Ca^{2+}-bound $SrtA_{\Delta N59}$ data, 94 out of a total of 98 quantifiable spins could be fit satisfactorily (the exceptions were Glu-95, Arg-99, Ile-123, and Gln-172). In the Ca^{2+}-bound $SrtA_{\Delta N59}$ analysis, Model 1 (S^2) was selected for 75 residues, 3 residues fit to model 2 (S^2 and τ_e), 12 residues fit to model 3 (S^2 and R_{ex}), 2 fit to model 4 (S^2, τ_e, and R_{ex}), and 6 residues fit to model 5 (S_f^2, S_s^2, and τ_e). Interestingly, in both Ca^{2+}-bound and apo-Ca^{2+} $SrtA_{\Delta N59}$, the relaxation data from Glu-95 and Ile-123 could not be fit to any model, suggesting that they undergo more complicated motions. The results of the model-free analysis for both conditions are provided in supplemental Tables S1 and S2. The average order parameters for apo-$Ca^{2+}$and Ca^{2+}-bound $SrtA_{\Delta N59}$ are 0.88 ± 0.14 and 0.89 ± 0.10, respectively. If only residues located in regions of regular secondary structure are considered, the order parameters are 0.943 ± 0.030 and 0.935 ± 0.016, for apo-$Ca^{2+}$and Ca^{2+}-bound $SrtA_{\Delta N59}$, respectively.

RESULTS AND DISCUSSION

Ca^{2+} Promotes Substrate Binding—To identify the step(s) at which Ca^{2+} stimulates catalysis, we monitored the *in vitro* activity of $SrtA_{\Delta N59}$ using an internally quenched fluorescent substrate analogue (*o*-aminobenzoyl-L-P-E-T-G-2,4-dinitrophenyl) (25). The $SrtA_{\Delta N59}$ mediated cleavage of the peptide bond between the threonine and glycine residues in this substrate results in an increase in fluorescence and can be used to monitor both hydrolysis and transpeptidation. The presence of Ca^{2+} stimulates both the hydrolytic and transpeptidation activities of $SrtA_{\Delta N59}$ (data not shown). Because both reactions differ only in the nucleophile used to resolve the acyl-intermediate, these results indicate that ion binding activates an early step in catalysis (*e.g.* sorting signal binding, activation of the Cys-184 thiol, or resolution of the enzyme-sorting signal thioacyl intermediate). To further pinpoint the step at which it acts, we monitored the hydrolytic activity of $SrtA_{\Delta N59}$ in the presence of varying amounts of Ca^{2+}. The hydrolysis reaction can be represented as in Reaction 1,

$$E + RCO\text{-}X \underset{k_4}{\overset{k_1}{\rightleftharpoons}} E \cdot RCO\text{-}X \xrightarrow[k_2]{XH} RCO\text{-}E \xrightarrow[k_4]{H_2O} E + RCO_2H$$

REACTION 1

where *E*, *E*·RCO-X, and RCO-*E* represent the free enzyme, the enzyme-bound to the sorting signal, and the acyl enzyme·substrate complex, respectively; RCO_2H and XH are the cleaved peptide and the free glycine, respectively; and k_1, k_{-1}, k_2, and k_4 are the rate constants describing their interconversion (25). Lineweaver-Burk plots of the hydrolysis data recorded at varying Ca^{2+} concentrations reveal a common $1/V_s$ intercept, indicating that the k_{cat} of the reaction is unaffected (Fig. 1*A*). It can also be concluded from this data that the values of k_2 and k_4 are independent of Ca^{2+}, because k_{cat} is defined as $k_2 * k_4/[k_2 + k_4]$. In contrast, the presence of Ca^{2+} clearly alters the Michaelis-Menten constant (K_m) of the reaction, because the slopes of the data are inversely proportional to $K_m * k_{cat}$, and the value of k_{cat} is independent of Ca^{2+}. Because K_m is defined as $[k_2 + k_{-1}]/k_1$, and k_2 is unchanged by Ca^{2+}, we conclude that Ca^{2+} stimulates $SrtA_{\Delta N59}$ activity by promoting substrate binding; it either increases k_1 or decreases k_{-1}.

The β3/β4 Pocket of $SrtA_{\Delta N59}$ Binds One Ca^{2+} Ion with Millimolar Affinity—Previously we used NMR to localize a Ca^{2+} binding site on $SrtA_{\Delta N59}$ to residues within the loop connecting strands $\beta3$ to $\beta4$ (the $\beta3/\beta4$ pocket) (17). However, the effects of Ca^{2+} are extensive, and, in addition to the $\beta3/\beta4$ pocket, dramatic chemical shift changes were observed in a large adjacent loop that connects strands $\beta6$ to $\beta7$ (the

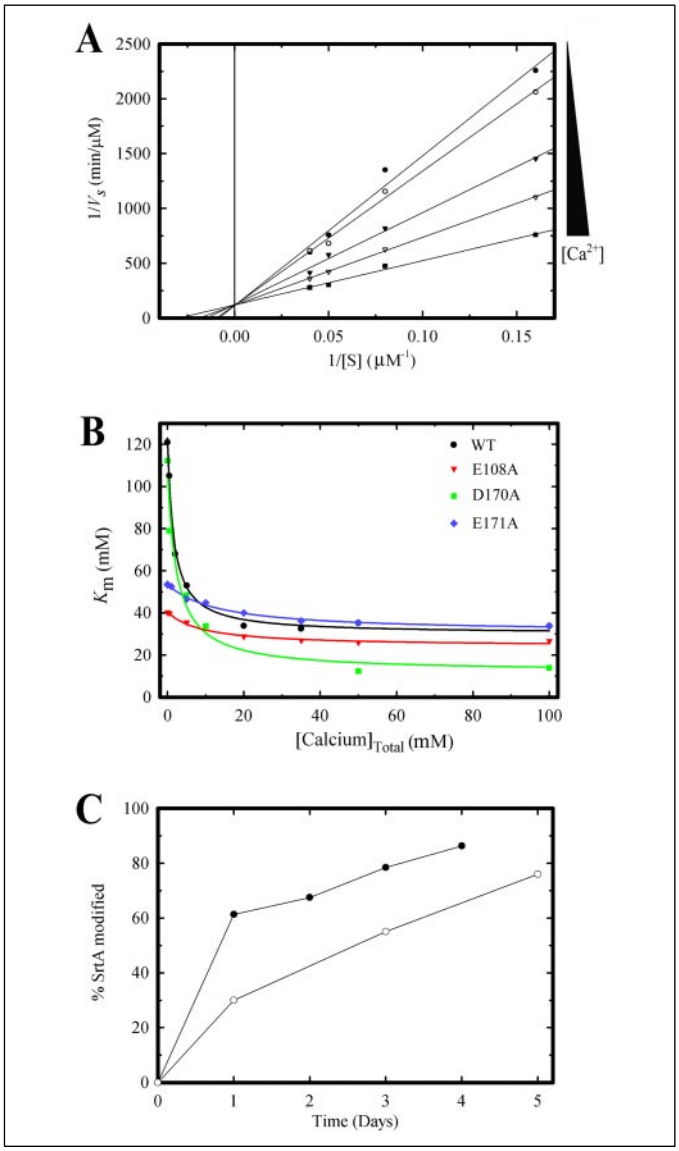

FIGURE 1. *A*, Lineweaver-Burk plot of wild-type $SrtA_{\Delta N59}$ activity at different concentrations of Ca^{2+}. Kinetic parameters were measured using a fluorescence resonance energy transfer assay monitoring the cleavage of a fluorescent peptide by wild-type $SrtA_{\Delta N59}$ at the following Ca^{2+} concentrations: 0 mM (●), 0.5 mM (○), 2 mM (▼), 5 mM (▽), and 20 mM (■). Increasing Ca^{2+} concentrations yielded lower K_m values. *B*, effects of Ca^{2+} on the K_m values of substrate hydrolysis by wild-type $SrtA_{\Delta N59}$ (*black* ●) and mutant $SrtA_{\Delta N59}$: E108A (*red* ▼), D170A (*green* ■), and E171A (*blue* ◆). The K_m values at various concentrations of Ca^{2+} were fit to Equation 2, yielding the dissociation constant (K_d) for Ca^{2+}, as shown in Table 1. *C*, graph depicting the effect of Ca^{2+} (20 mM) on the rate of $SrtA_{\Delta N59}$ modification by a peptidyl-sulfhydryl compound containing the sorting signal sequence LPAT. The compound modifies SrtA by forming a disulfide bond with Cys-184, changing the retention time of the protein on reverse phase-high-performance liquid chromatography. The percentage of $SrtA_{\Delta N59}$ modified was calculated by integrating the peaks corresponding to modified and unmodified $SrtA_{\Delta N59}$ in the chromatogram in the presence (●) and absence (○) of Ca^{2+}.

β6/β7 loop). Because many of the perturbed residues in the β6/β7 loop are far away from the β3/β4 pocket, their shift changes cannot be caused by direct effects (see Fig. 4*B* of Ref. 17). Instead, either additional ions bind to the β6/β7 loop, and/or ion binding to the β3/β4 pocket triggers a conformational rearrangement that perturbs the chemical shifts of residues within the β6/β7 loop. Because our previous work did not distinguish between these two possibilities, we precisely localized the divalent ion binding site(s) on $SrtA_{\Delta N59}$ by titrating the enzyme with Mn^{2+} and monitoring its ^1H-^{15}N HSQC NMR spectrum. It is expected that Mn^{2+} will bind to the same site(s) as Ca^{2+}, because they are both divalent ions and because Mn^{2+} also stimulates enzyme activity (albeit to a lesser extent) (17). Importantly, titrations with Mn^{2+} enable precise definition of the ion-binding pocket, because it is paramagnetic, such that even at sub-saturating levels it selectively broadens only nearby protein resonances (46). A series of ^1H-^{15}N HSQC spectra of apo-Ca^{2+} $SrtA_{\Delta N59}$ were recorded in the presence of varying concentrations of Mn^{2+} (0, 25, 50, 100, 200, 500, and 1000 μM). When 50 μM Mn^{2+} is added, several ^1H-^{15}N resonances within the β3/β4 pocket selectively disappear (Fig. 2*B*), whereas at higher Mn^{2+} concentrations, residues adjacent to surface-exposed acidic side chains exhibit nonspecific line broadening (Fig. 2*A*). Only a single Ca^{2+} ion binds to the β3/β4 pocket as a superposition of a series of ^1H-^{15}N HSQC spectra recorded with varying amounts of Ca^{2+} reveals linear changes in the protein's chemical shifts (Fig. 2*C*), whereas non-linear changes are expected if multiple ions were to bind (47). Moreover, an analysis of a plot of the Ca^{2+} chemical shift changes *versus* $[Ca^{2+}]/[SrtA_{\Delta N59}]$ reveals a binding ratio of 1:1 (data not shown). Taken together, these data show that the aforementioned β3/β4 pocket binds to a single Ca^{2+} ion and that it is the only high affinity ion binding site on sortase. The extensive Ca^{2+}-dependent chemical shift changes in the β6/β7 loop can therefore be attributed to a structural rearrangement within or nearby this region (Fig. 3*A*).

The affinity of the β3/β4 pocket for Ca^{2+} has not been determined quantitatively and is needed for NMR dynamics and kinetic studies. Values for the dissociation constant were therefore estimated from the Ca^{2+} dependence of the apparent K_m (Fig. 1*B*) using Equation 2,

$$K_m = K_{m_{max}} - \left(\frac{(K_{m_{max}} - K_{m_{min}})[Ca^{2+}]}{[Ca^{2+}] + K_d} \right) \qquad \text{(Eq. 2)}$$

where $K_{m_{max}}$ and $K_{m_{min}}$ are the K_m values of the enzyme in the absence and presence of Ca^{2+}, respectively, and K_d is the dissociation constant for ion binding (48). Curve fitting of the data reveal that saturating amounts of Ca^{2+} cause a 4.2-fold decrease in the K_m from 121 μM to 33 μM and that the ion binds with a K_d of 1.6 ± 0.3 mM. A similar binding constant of 2.2 ± 0.5 mM is obtained by directly curve fitting the Ca^{2+} dependence of the chemical shift data (Fig. 2*D*). Because the concentration of Ca^{2+} is ~2.5 mM in human serum, these results suggest that about half of the SrtA molecules on the surface of *S. aureus* are Ca^{2+}-bound during bacteremia. However, this is likely an underestimate because the binding of the substrate and ion to the protein presumably forms a closed thermodynamic cycle, which necessitates that the substrate-bound enzyme exhibit ~4-fold higher affinity for Ca^{2+} as compared with the substrate-free enzyme (49).

Ca^{2+} Does Not Directly Interact with the Sorting Signal—NMR, x-ray, and targeted mutagenesis studies have localized the sorting signal binding site to a large hydrophobic surface immediately adjacent to the ion-binding pocket (18, 22), raising the possibility that direct ion-substrate interactions stimulate catalysis. An inspection of the recently determined x-ray structure of a Cys-184 → Ala mutant of $SrtA_{\Delta N59}$ ($^{C184A}SrtA_{\Delta N59}$) bound to a LPETG peptide reveals that the side chain of the central glutamic acid in the peptide is nearest to the ion-binding pocket (18). However, this structure cannot reveal whether the ion directly contacts the substrate, because it was solved in the absence of Ca^{2+}. Because the stimulatory effect of divalent cations has only been demonstrated using a fluorogenic substrate that also has glutamic acid at this position, we wondered whether acidic residues at the central position within the substrate were needed for Ca^{2+} stimulation. To answer this question, the effect of Ca^{2+} on the rate of enzyme modifi-

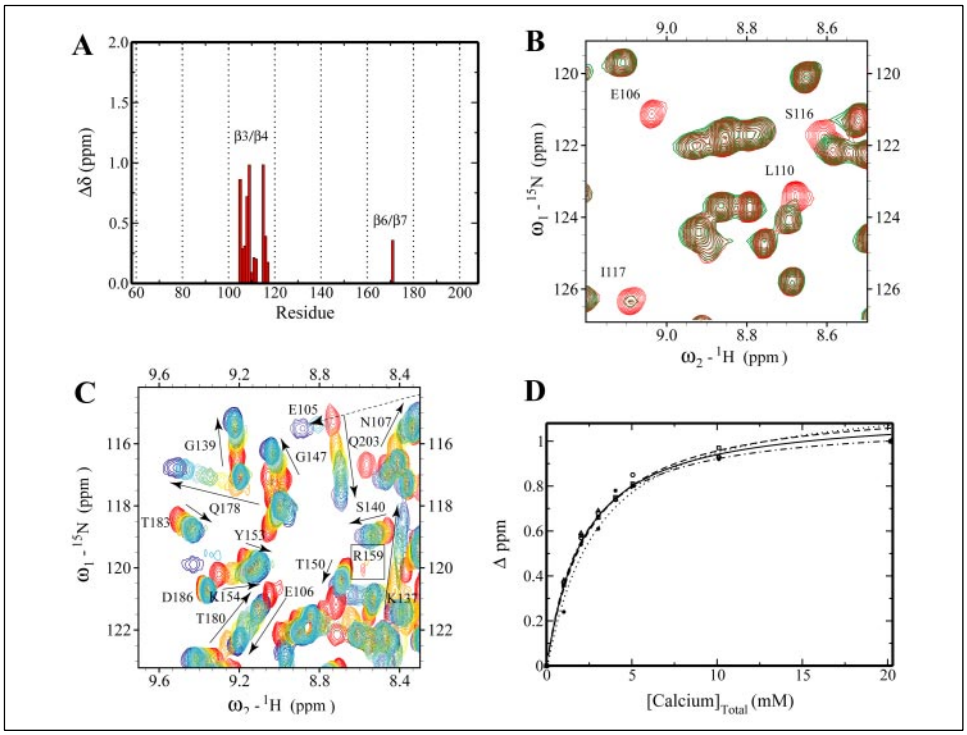

FIGURE 2. *A*, a histogram showing residues that are broadened beyond detection due to the addition of paramagnetic Mn^{2+}. The magnitude of compound ^{15}N-^{1}H chemical shift changes ($\Delta\delta$) for backbone amide resonances caused by the addition of Ca^{+} is depicted from our original perturbation study (17), where $\Delta\delta = \sqrt{(\Delta\delta_H)^2 + (\Delta\delta_N/6.49)^2}$. *B*, selected portion of two ^{1}H-^{15}N HSQC spectra acquired in the absence (*red*) and presence (*green*) of 50 μM Mn^{2+}. Peaks shown only in *red* with no trace of overlapping *green* disappear beyond detection and are predominantly localized to the Ca^{2+}-binding pocket. A small number of residues distant from the Ca^{2+}-binding surface also broaden outward, but these don't show any significant changes in their chemical shifts in the presence and absence of Ca^{2+} and therefore represent Mn^{2+}-specific interactions. *C*, overlay of eight ^{1}H-^{15}N HSQC spectra acquired at different Ca^{2+} concentrations ranging from 0 mM (*red*), 1 mM (*orange*), 2 mM (*yellow*), 3 mM (*green*), 4 mM (light green), 5 mM (light blue), 10 mM (cyan), to 20 mM (*blue*). The *black arrows* indicate the linearity of peak movement, which is clear evidence for a single Ca^{2+} ion-binding event. Resonance assignments at both 0 mM and 20 mM Ca^{2+} were independently verified by triple resonance experiments, and the resulting chemical shift differences are shown in *A*. *D*, representative $SrtA_{\Delta N59}$-Ca^{2+} binding profiles constructed from the backbone amide chemical shift changes observed from the series of HSQC spectra shown in panel *C*. Data for Asn-107 (*circle* and *solid line*); Glu-108 (*square* and *dashed line*); Asp-112 (*triangle* and *dash-dot line*); and Glu-171 (*asterisk* and *dotted line*) is shown here. The *symbols* represent experimental data while the *lines* represent curve fits performed using the program CaLigator (68). The deduced Ca^{2+} binding constant has a high precision for residues from the Ca^{2+} binding surface with an average dissociation constant, $K_d = 2.21 \pm 0.51$ mM. Thirteen residues were used to estimate this K_d value: Asn-107, Glu-108, Ser-109, Leu-110, Asp-112, Ile-115, Ser-116, Gly-167, Val-168, Leu-169, Asp-170, Glu-171, and Gln-172.

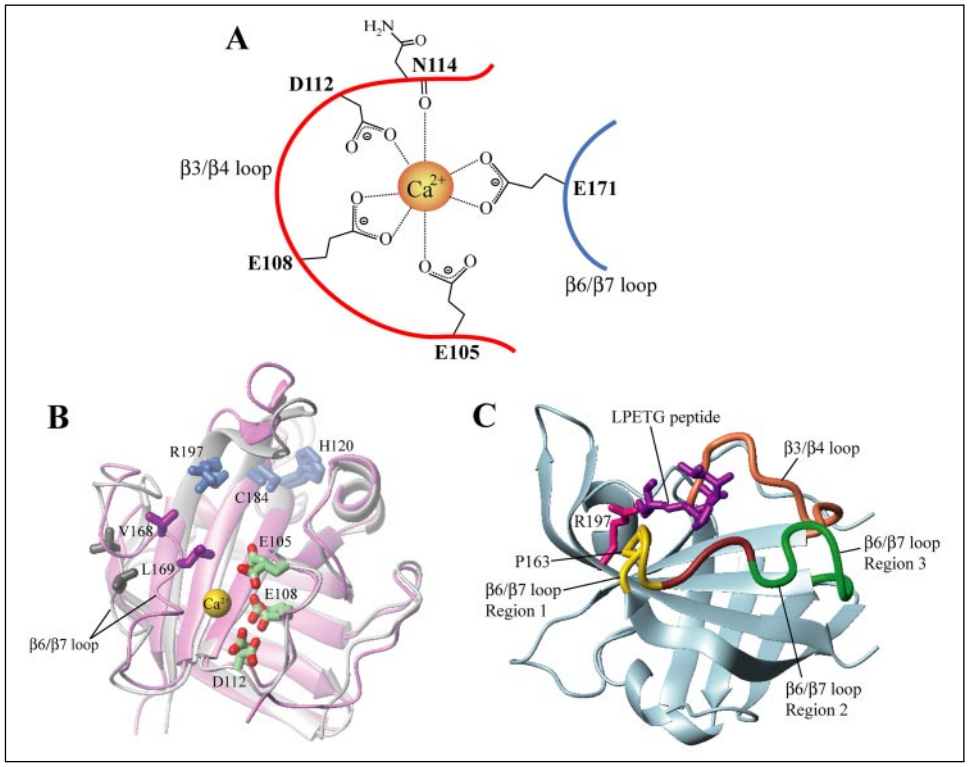

FIGURE 3. *A*, schematic showing Ca^{2+} ion coordination by $SrtA_{\Delta N59}$. Ca^{2+} ion binding site(s) predicted previously (17) was precisely localized by Mn^{2+} titration experiments monitoring its ^{1}H-^{15}N HSQC NMR spectra and by inspection of the NMR solution structure of the Ca^{2+}-bound form of the protein (PDB accession code: 1IJA). These new data indicate that the previously predicted $\beta3/\beta4$ pocket binds to a single Ca^{2+} ion, and it is the only high affinity Ca^{2+} binding site on $SrtA_{\Delta N59}$. *B*, overlay of the NMR (*pink*) and crystal (*gray*) structures solved in the presence and absence of Ca^{2+}, respectively. This figure shows that only the structure of the loop connecting strands $\beta6$ to $\beta7$(the $\beta6/\beta7$ loop) is dramatically affected upon Ca^{2+} binding. The side chains of Val-168 and Leu-169 (within the $\beta6/\beta7$ loop) are colored *pink* and *gray* in the NMR and crystal structures, respectively. The side chains of active site residues and Ca^{2+}-ligating residues are shown in *blue* and *green*, respectively. *C*, a ribbon diagram of the crystal structure of the complex between $^{C184A}SrtA_{\Delta N59}$ and a peptide containing the sequence LPETG. Regions 1–3 of the $\beta6/\beta7$ loop are colored *yellow*, *red*, and *green*, respectively. The $\beta3/\beta4$ pocket, which is responsible for chelating the Ca^{2+} ion, is shown in *light brown*. The LPETG peptide is shown in *purple*, and the side chains of Pro-163 and the catalytically important Arg-197 are shown in *yellow* and *pink*, respectively.

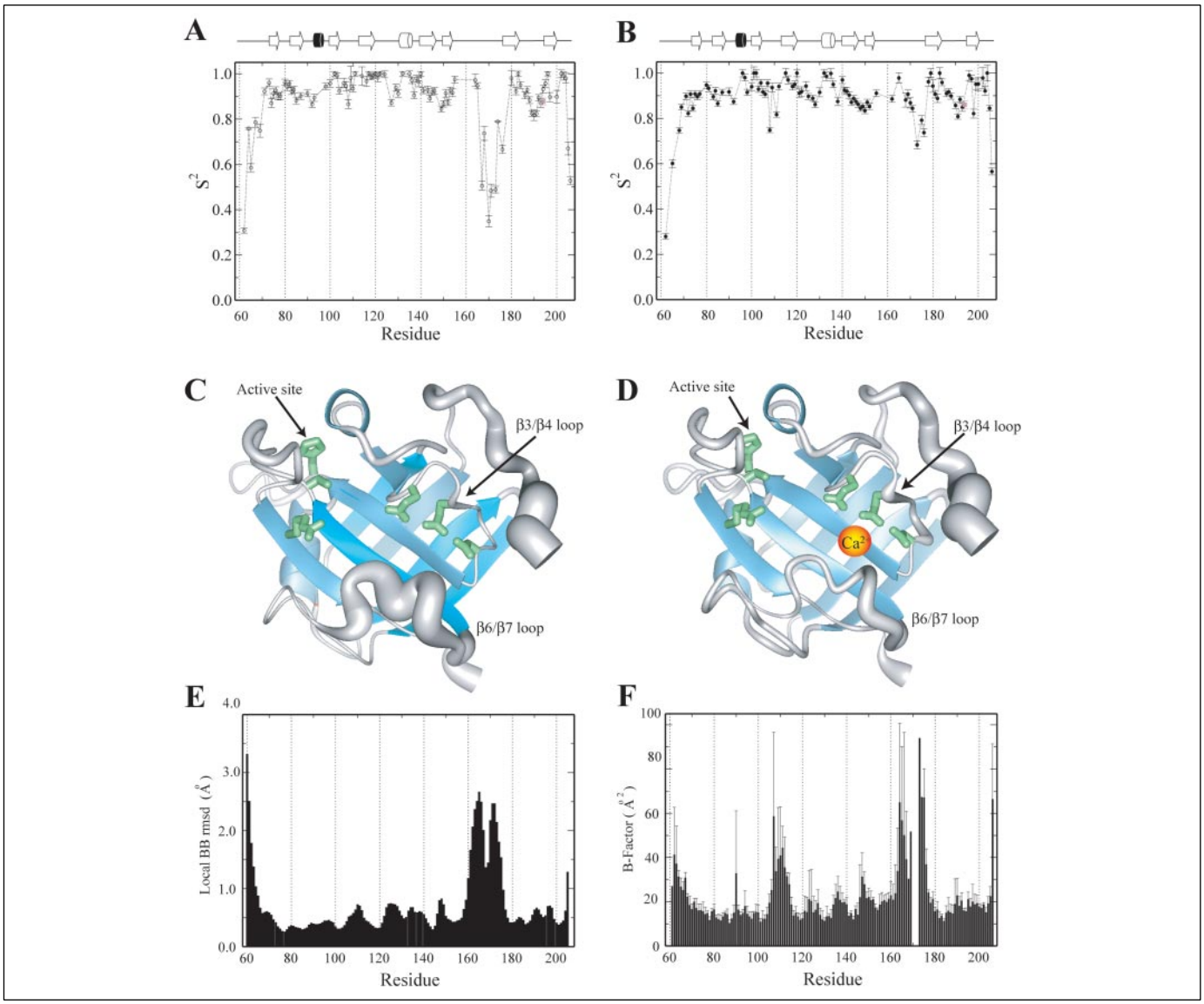

FIGURE 4. **Ca^{2+} binding quenches fast picosecond time-scale motions near the ion binding pocket.** The S^2 values for the apo-Ca^{2+} (*A*)- and Ca^{2+} (*B*)-bound forms of $SrtA_{\Delta N59}$ are plotted as a function of residue number. A schematic of the secondary structural elements is shown *above each panel*. The average order parameter for apo-Ca^{2+} $SrtA_{\Delta N59}$ is 0.88 ± 0.14, whereas for Ca^{2+}-bound $SrtA_{\Delta N59}$, it is 0.89 ± 0.10. The order parameters for each form are mapped onto ribbon diagrams of $SrtA_{\Delta N59}$ in *panels C* (apo-Ca^{2+}) and *D* (Ca^{2+}-bound). The width of each tube connecting the secondary structural elements is inversely proportional to the size of the S^2 value (*i.e.* wider regions indicate more flexible parts of the protein). Because residues in regular secondary structure exhibited uniformly high S^2 values, they are represented in *blue* by *arrows* (β sheets) and coils (α helices) of uniform size. The catalytic (His-120, Cys-184, and Arg-197) and Ca^{2+} binding side chains are displayed in *green*. The relaxation data are mapped onto the coordinates of the NMR structure of Ca^{2+}-bound protein. *E*, representative histogram of the root mean square deviations of the local backbone assignments of the $SrtA_{\Delta N59}$ solution structure (17). *F*, representative histogram of *B*-factors of the $SrtA_{\Delta N59}$ crystal structure (18).

cation by a peptidyl-sulfhydryl compound containing the sorting signal sequence LPAT was tested (benzoyloxycarbonyl-Leu-Pro-Ala-Thr, with the C-terminal carbonyl group of Thr replaced with -CH_2-SH). This compound modifies $SrtA_{\Delta N59}$ by forming a disulfide bond with Cys-184 within the active site (22). As shown in Fig. 1*C*, the presence of Ca^{2+} increases the rate at which it modifies the enzyme, presumably by promoting its binding similar to the substrate. Because the hydrophobic alanine side chain cannot serve as a ligand for Ca^{2+}, we conclude that interactions from the central position in the substrate are not required for the stimulatory effect of Ca^{2+}. This finding is substantiated by recent studies by the McCafferty group that have demonstrated that peptide substrates in which the glutamic acid is replaced by a range of amino acids are still effectively cleaved by SrtA (50). Moreover, we have recently determined the solution structure of the sortase·peptide complex in the presence of Ca^{2+}, which shows that the substrate and ion to do not directly interact with one another.[4]

Nitrogen-15 Relaxation Measurements—The proximity of the $\beta 6/\beta 7$ loop to the active site and its extensive Ca^{2+}-dependent chemical shift changes argue that it undergoes an ion-induced structural change that promotes substrate binding. Interestingly, structural data also suggest that the loop is flexible, because in both the NMR and x-ray structures, its residues exhibit elevated root mean square deviations (Fig. 4*E*) and *B*-factors (Fig. 4*F*), respectively (17, 18). This raises the interesting possibility that Ca^{2+} also modulates the flexibility of the loop to stimulate substrate binding. Because nothing is known about the conformational

[4] M. T. Naik, N. Suree, U. Ilangovan, C. K. Liew, W. Thieu, D. O. Campbell, J. J. Clemens, M. E. Jung, and R. T. Clubb, unpublished observation.

TABLE 1

Kinetic parameters of wild-type and mutant sortases

Triplicate data sets for each experiment were used to calculate the steady-state velocity (V_s) at different *o*-aminobenzoyl-LPETG-dinitrophenyl and Ca^{2+} concentrations for each enzyme as described previously (25). K_m and V_{max} values were determined by double-reciprocal plot of the substrate dependence of V_s. Dissociation constants (K_d) for Ca^{2+} binding were calculated by curve fitting of the apparent K_m data using Equation 2. Relative affinity is the K_d ratio comparing to the wild-type enzyme.

Enzyme	K_d	Relative affinity	Relative affinity (NMR)[a]	V_{max}	k_{cat}
	mM			$\mu M\ min^{-1}$	min^{-1}
Wild-type	1.6 ± 0.23	1	1	$8.5 \times 10^{-3} \pm 2.2 \times 10^{-4}$	$5.7 \times 10^{-3} \pm 1.5 \times 10^{-4}$
E108A	9.0 ± 2.4	0.18	N/A[b]	$1.3 \times 10^{-4} \pm 6.7 \times 10^{-6}$	$8.5 \times 10^{-5} \pm 4.5 \times 10^{-6}$
D170A	2.4 ± 0.82	0.67	1.4	$8.7 \times 10^{-3} \pm 1.3 \times 10^{-4}$	$5.8 \times 10^{-3} \pm 8.6 \times 10^{-4}$
E171A	13.3 ± 1.9	0.12	0.02	$1.8 \times 10^{-3} \pm 3.1 \times 10^{-4}$	$1.2 \times 10^{-3} \pm 2.1 \times 10^{-4}$

[a] Determined by curve fitting of the Ca^{2+}-dependent chemical shift perturbation as described under "Materials and Methods."
[b] The Ca^{2+}-dependent chemical shift perturbation has slight or no change, indicating a very weak binding of the mutant enzyme to Ca^{2+}.

dynamics of any sortase enzyme and there is no quantitative relationship between structural parameters and mobility, we rigorously defined the Ca^{2+} dependence of motions in $SrtA_{\Delta N59}$ by measuring the rates of longitudinal (R_1) and transverse (R_2) relaxation, as well as $\{^1H\}$-^{15}N NOE values of the backbone nitrogen-15 atoms. Two samples of $SrtA_{\Delta N59}$ in different states of ligation were investigated: (i) an apo-Ca^{2+} form (50 mM Tris-HCl, 100 mM NaCl, 3 mM dithiothreitol, 7% D_2O, and 0.01% NaN_3; pH 6.2) and (ii) a Ca^{2+}-bound form (conditions identical to the apo-Ca^{2+} SrtA form, but with 20 mM Ca^{2+} present). The relaxation data were then interpreted using the Modelfree formalism to gain insights into the magnitudes and time scales of motion. Graphs showing the relaxation data as a function of residue number are shown in supplemental Fig. S1 and tables listing the values of the Modelfree parameters (S^2, τ_e, and R_{ex}) are provided as supplemental Tables S1 and S2.

Residues in the β6/β7 Loop Transiently Participate in Ion Binding—The coordinates of the β6/β7 loop are poorly defined in both the NMR and x-ray structures of the enzyme (Fig. 4, *E* and *F*). However, its residues can be divided into three sections based on their positioning relative to the active and ion binding sites, and their dynamics properties were revealed by NMR (Fig. 3*C*). At its N-terminal end, residues Lys-162 to Val-166 (region 1) ascend from the body of the protein so as to position the ring of Pro-163 immediately adjacent to the catalytic side chain of Arg-197. Residues Gly-167 to Asp-170 (region 2) then form the substrate-contacting surface and are followed by residues Asp-170 to Asp-176 (region 3), which are positioned proximal to the ion-binding site in the β3/β4 pocket. From the relaxation data analysis, the S^2 parameter is calculated, which gives a concise account of each the mobility of N–H bond vector on the picosecond time scale; it ranges from 0 to 1, with a value of 1 indicating that the amide is completely immobilized. Inspection reveals that only the β6/β7 loop exhibits significant Ca^{2+}-dependent changes in its dynamics (Fig. 4, compare *A* and *B*). When the S^2 data are mapped onto the structure, it is apparent that residues in regions 2 and 3 of the β6/β7 loop become partially immobilized when the ion is bound (in Fig. 4, *C* and *D*, the thickness of the chain is correlated with increased mobility in the apo-Ca^{2+} and Ca^{2+}-bound forms, respectively). Interestingly, residual picosecond motions in the β6/β7 loop persist even in the presence of Ca^{2+}, implying that it transiently binds Ca^{2+}. This may explain the weak affinity of the protein for the ion (Figs. 1*B* and 2*D*) and the observed disorder in the β6/β7 loop in the NMR structure of the Ca^{2+}-bound enzyme.

Glu-171 in the β6/β7 Loop Is Important for Ca^{2+} Binding—Because the NMR data indicate that the β6/β7 loop becomes immobilized when the ion is present, it seems likely that it contains one or more residues that directly contact the ion in the β3/β4 pocket. Because the coordinates of the β6/β7 loop are poorly defined in both the NMR and crystal structures, it is not possible to unambiguously identify contacts from it to the ion (Fig. 4, *E* and *F*). However, as previously noted, the side chain of Glu-171 within the β6/β7 loop is a likely candidate for ion binding, because in several of the conformers of the NMR structure of Ca^{2+}-bound $SrtA_{\Delta N59}$ it is poised to interact with the ion. This is also consistent with the finding that the adjacent backbone amides of the nearby residues Leu-169 and Asp-170 experience the largest ion-dependent changes in their S^2 parameters and chemical shifts, respectively.

To determine if ion contacts from Glu-171 act to immobilize the β6/β7 loop, the Ca^{2+} binding properties of three single amino acid mutants of $SrtA_{\Delta N59}$ were tested. Each mutant replaces potential ion binding acidic side chains with alanine and target residues that are located in the β6/β7 loop (Asp-170 → Ala and Glu-171 → Ala) or the β3/β4 ion binding pocket (Glu-108 → Ala). All of the mutant proteins remain folded as judged by their NMR spectrum (data not shown) and retain enzymatic activity (Table 1). The Ca^{2+} binding properties of the mutants were assessed by measuring the Ca^{2+} dependence of their enzymatic activity as previously described for the wild-type protein. As shown in Fig. 1*B*, the K_m values for the wild-type and D170A mutant proteins show a similar dependence on Ca^{2+}, indicating that Asp-170 within the β6/β7 loop does not bind Ca^{2+}. In contrast, both the E108A and E171A mutants show reduced Ca^{2+} sensitivity (Fig. 1*B*). The E108A mutant serves as a positive control, because it has been shown to unambiguously interact with the ion based on Mn^{2+} titration data (Fig. 2*A*). The finding that it and E171A have similar effects on catalysis suggests that Glu-171 within the β6/β7 loop contacts the ion. Most importantly, fits of the Ca^{2+} dependence of the K_m values to Equation 2 reveal that the E108A and E171A mutants bind Ca^{2+} with 10-fold lower affinity than the wild-type or D170A proteins. To verify the relative Ca^{2+} binding affinities of the mutants, NMR was also used to directly monitor ion binding. As shown in Table 1, affinity measurements by NMR gave similar results as the kinetic analysis and indicate that Glu-108 in the β3/β4 pocket and Glu-171 in the β6/β7 loop are involved in binding the ion, whereas Asp-170 is not. These data are consistent with ion contacts from Glu-171 acting to stabilize ion binding.

Ion Binding Redistributes Slow Motions toward the Active- and Substrate-binding Sites—Protein motions on micro- to millisecond time scales are important for enzymatic catalysis and ligand recognition (51, 52). Because the Modelfree approach only characterizes these processes indirectly as a contribution to transverse relaxation in the form of the R_{ex} term, we performed relaxation-compensated CPMG (rc-CPMG) experiments to directly investigate these motions (53, 54). Slow timescale conformational rearrangements in $SrtA_{\Delta N59}$ are revealed by the data shown in Fig. 5 (*A* and *B*), which displays plots of the R_{ex} terms derived from the Modelfree analysis (*open bars*) and the difference in transverse relaxation rates when long (τ_{cp} = 4 ms) and short (τ_{cp} = 1 ms) inter-pulse delays are used in the CPMG sequence (*filled circles*). Positive differences in the transverse relaxation rates are indicative of slow chemical exchange events and are in good qualitative agreement with the Modelfree data.

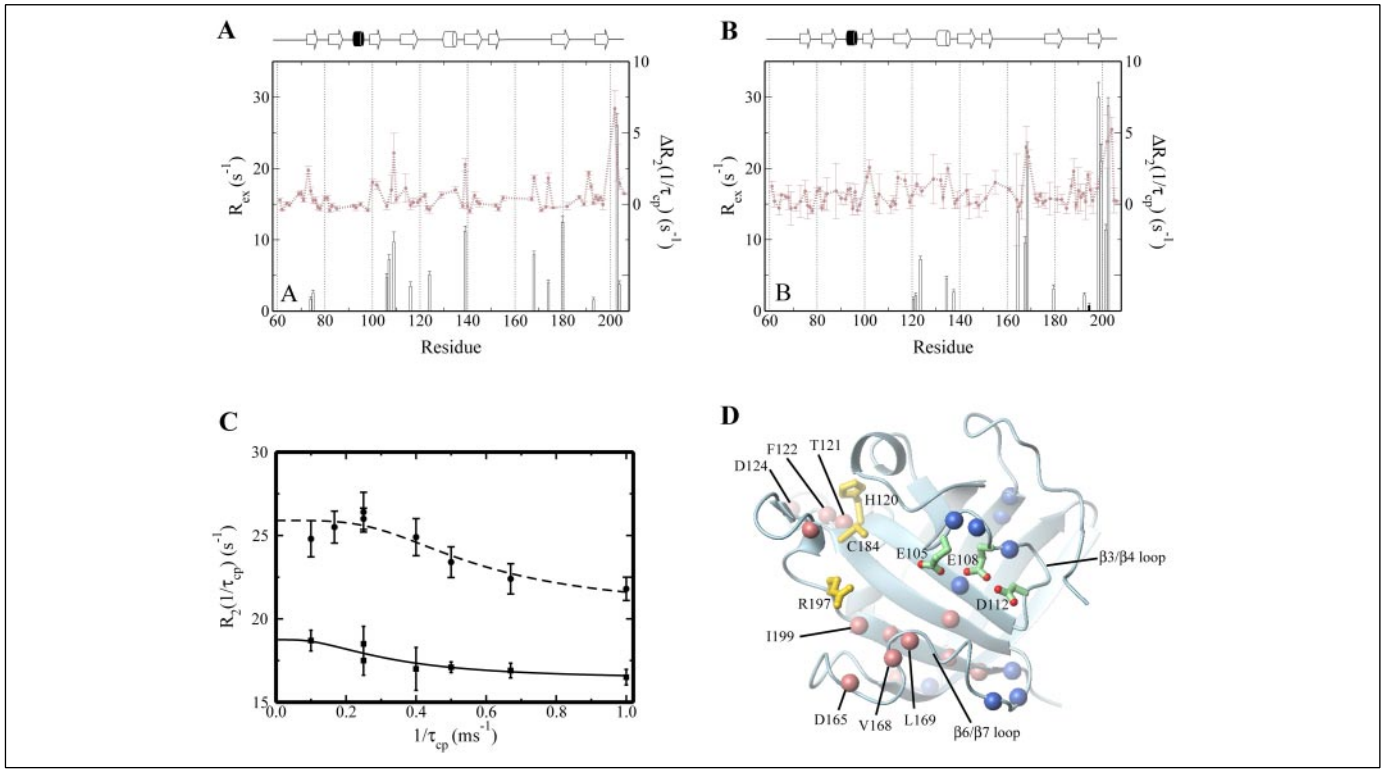

FIGURE 5. **Observed milli- to microsecond Ca^{2+}-dependent dynamics in $SrtA_{\Delta N59}$.** The R_{ex} values in the apo-Ca^{2+} (*A*)- and Ca^{2+} (*B*)-bound forms of $SrtA_{\Delta N59}$ are plotted as a function of residue number. The data are presented as *bar graphs* with the *errors* indicated (R_{ex} values $>1\ s^{-1}$ are generally considered reliable). The *panels* also show the results of rc-CPMG experiments that serve to verify the existence of conformational exchange. Plotted as *gray circles* is the qualitative difference, $\Delta R_2(1/\tau_{cp})$, in the measured transverse relaxation rates when $\tau_{cp} = 4$ ms and $\tau_{cp} = 1$ms. *C*, dispersion curves generated from the rc-CPMG experiment. Experimentally determined $\Delta R_2(1/\tau_{cp})$ rate constants were fitted as a function of $1/\tau_{cp}$ using Equation 3. Data are shown for two residues positioned immediately adjacent to the Ca^{2+}-binding pocket: Glu-108 (*square* and *solid line*) and Ser-109 (*circle* and *dashed line*) where the *symbols* represent experimental data and the *lines* represent their fits to the equation. *D*, the redistribution of R_{ex} terms toward active- and substrate-binding sites when Ca^{2+} is present. The data from *panel A* have been mapped onto the structure of $SrtA_{\Delta N59}$, with *blue* and *red spheres* denoting protein residues that exhibit R_{ex} terms in the absence and presence of Ca^{2+}, respectively. Some residues exhibit R_{ex} terms in both the presence and absence of Ca^{2+} and are also indicated by a *red sphere* (residues Asp-124, Ala-135, Val-168, Thr-180, Val-193, Ala-202, and Thr-203).

The rc-CPMG data indicate that Ca^{2+} binding induces slow biologically relevant motions in the active site. In the absence of Ca^{2+}, residues exhibiting slow motional dynamics are evenly distributed throughout the primary sequence (Fig. 5*D*, *blue spheres*, and supplemental Table S1). The exception is the C-terminal portion of the $\beta6/\beta7$ loop near the ion, which in addition to fast picosecond motions, is in flux on slower time scales prior to Ca^{2+} binding (residues within (Gly-174 and Asp-176) and underneath (Ala-202, Thr-203, and Glu-204) this portion of the loop exhibit R_{ex} values). In contrast, in the Ca^{2+}-bound form, a spike in R_{ex} values was observed in region 2 of the $\beta6/\beta7$ loop (Fig. 5*D*, *red spheres*; residues Asp-165, Val-168, and Leu-169). These motions are likely triggered by an ion-induced movement of almost the entire loop, because all of it exhibits Ca^{2+}-dependent chemical shift changes (Fig. 4*B* of Ref. 17). Interestingly, a general redistribution of slow motions toward the active site occurs upon ion binding, because significant R_{ex} terms are also observed in residues Thr-121, Phe-122, and Asp-124, and in Ile-199, which immediately follow the catalytically essential His-120 and Arg-197 side chains (Fig. 5*D*). These motions may be correlated with the structural rearrangements that are required to catalyze hydrolysis. Interestingly, residues in region 2 form the substrate binding site in the crystal structure of the complex. This suggests that Ca^{2+}-triggered slow motions in this part of the loop may facilitate the adaptive recognition of the sorting signal.

Ion Binding and Active Site Motions Occur on Similar Time Scales—Our results clearly illustrate that Ca^{2+} acts to quench motions within the $\beta6/\beta7$ loop. Although the mutagenesis data suggest that ion contacts from Glu-171 immobilize the loop, we sought further support for this model by rigorously assessing the rate of slow protein motions and ion binding. If active site dynamics were coupled to Ca^{2+} binding via ion contacts from Glu-171, we reasoned that the rate of these conformational fluctuations would be similar. To investigate this issue, we quantified conformational exchange rates by performing rc-CPMG experiments on a new sample of $SrtA_{\Delta N59}$ containing 20 μM Ca^{2+} (3.2 mM $SrtA_{\Delta N59}$, 20 μM Ca^{2+}, 50 mM Tris-HCl, 100 mM NaCl, 3 mM dithiothreitol, 7% D_2O, and 0.01% NaN_3, pH 6.20). This enables a more accurate interpretation of the NMR data, because the exact populations of the ion-free and -bound forms of SrtA can be determined (assuming a $K_d = 2.2$ mM, this sample is composed of 99.2% and 0.08% equilibrium populations of the apo-Ca^{2+} and Ca^{2+}-bound $SrtA_{\Delta N59}$, respectively). According to Ishima and Torchia (55), under conditions similar to ours, in which the populations of the interchanging conformers are dramatically skewed, the phenomenological transverse relaxation rate $R_2(1/\tau_{cp})$ for all time scales is given by Equation 3,

$$R_2(1/\tau_{cp}) = R_2(1/\tau_{cp} \rightarrow \infty) + \left(\frac{p_s p_c \Delta\omega^2 k_{ex}}{k_{ex}^2 + \sqrt{p_s^2 \Delta\omega^4 + \frac{144}{\tau_{cp}^4}}} \right) \quad \text{(Eq. 3)}$$

where $\Delta\omega$ is the chemical shift difference between the two exchanging populations, k_{ex} is the rate of exchange, τ_{cp} is the delay between 180 degree pulses in the experiment, and p_S and p_C are the populations of the apo-Ca^{2+}

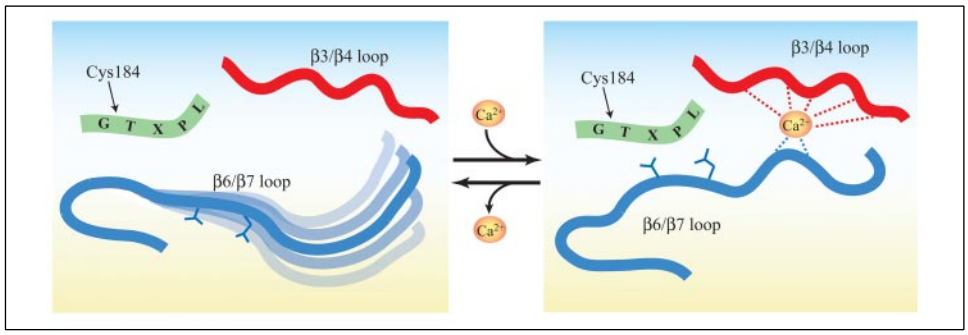

FIGURE 6. **Loop closure model describing how Ca^{2+} modulates the sorting signal binding site on SrtA.** The *panel* on the *left* shows SrtA in the absence of Ca^{2+}, emphasizing that the substrate contacting side chains of Val-168 and Leu-169 are removed from the active site, and the loop is more flexible. The panel on the *right* shows how contacts from the $\beta6/\beta7$ loop to the Ca^{2+} ion bound in the $\beta3/\beta4$ site act to immobilize and reposition the loop for favorable contacts to the LPXTG sorting signal.

and Ca^{2+}-bound forms of $SrtA_{\Delta N59}$, respectively. To extract k_{ex} and $\Delta\omega$, we measured dispersion curves in which R_2 was determined using different τ_{cp} delays (representative data are provided in Fig. 5*C*). A total of ten residues exhibited adequate dispersion curves that enabled the extraction of their exchange parameters through Jackknife simulations (supplemental Table S3). Eight of the ten residues serve as probes for the effects of Ca^{2+} binding, because they are positioned in the ordered portion of the ion-binding pocket (Glu-108 and Ser-109), underneath the ion-binding pocket (Ala-202 and Glu-204), or in the $\beta6/\beta7$ loop (Val-168 and Gly-174). The rate of dissociation of the ion from the protein (k_{off}) is calculated to be 1152 ± 114 s^{-1}, if data solely from residues Glu-108 and Ser-109 are used. Because they reside in the rigid ion-binding $\beta3/\beta4$ pocket, it can be assumed that their k_{ex} values strictly reflect the Ca^{2+}-binding event ($k_{ex} = k_{off} + k_{off}[Ca^{2+}_{free}]$) (56). Interestingly, similar k_{ex} values are observed for residues Val-168 and Gly-174 within the $\beta6/\beta7$ loop, and the Ca^{2+}-dependent chemical shift changes predicted from the relaxation data are similar to their experimentally measured values (supplemental Table S3). Although this analysis assumes a simplified two-state mode for the dynamics, the results suggest that the time scale of motions occurring within the substrate binding surface are similar to the rate of ion exchange from the protein.

Interpretation of the Dynamics Data—The Mn^{2+}, NMR relaxation, and mutagenesis data reported herein, and previous chemical shift mapping studies, indicate that ion binding to the $\beta3/\beta4$ pocket causes the $\beta6/\beta7$ loop to undergo a structural change that reduces its mobility. Because the coordinates of the $\beta6/\beta7$ loop are poorly defined in both the crystal and NMR structures (Fig. 4, *E* and *F*) no detailed structural framework exists to interpret the dynamics data. However, gross features of these structures suggest that the loop toggles between two basic states that differ in their overall positioning relative to the body of the protein. In the NMR structure solved in the presence of Ca^{2+}, the loop is partially immobilized and tethered to the body of the protein in a "closed" state. The NMR data strongly support this conformation, as the side chains of Val-168 and Leu-169 in the loop are unambiguously positioned adjacent to the active site (Fig. 3*B*) by several NOE cross-peaks between these residues and atoms in the underlying beta sheet (data not shown). A closed state for the loop in the presence of Ca^{2+} is also compatible with the results of our mutagenesis studies, which show that an acidic side chain positioned adjacent to these residues (Glu-171) presumably closes the loop by contacting Ca^{2+} (Figs. 1*B* and 3*A*). The disorder of the $\beta6/\beta7$ loop observed in the NMR structure can be attributed to residual slow conformational dynamics of this region detected by the rc-CPMG experiments and to the prevalence of hydrophilic side chains whose degenerate chemical shifts make it notoriously difficult to identify distance restraints. In the absence of Ca^{2+} NMR data indicate that the $\beta6/\beta7$ loop is more flexible (Fig. 4, *A* and *B*). The available structural data are compatible with this finding, because in the crystal structure solved in the absence of Ca^{2+}, regions 2 and 3 of the loop form a flap that adopts an "open" conformation in which the hydrophobic side chains of Val-168 and Leu-169 are rotated away from the body of the protein. Interestingly, in the three molecules of the asymmetric unit the flap adopts very distinct structures, or is missing electron electronic density. This variability and our observation of large amplitude picosecond time-scale motions in these residues suggest that in the absence of Ca^{2+} regions 2 and 3 adopt a variety of rapidly interchanging conformers in which the flap is primarily untethered from the body of the protein. The NMR data indicate the $\beta6/\beta7$ loop in the absence of substrate is mobile regardless of ion occupancy. In the spectra of the apo-Ca^{2+} and Ca^{2+}-bound forms, extensive line broadening is observed in the beta bulge structure at the end of strand $\beta6$, which is positioned below the flap (regions 2 and 3). Even after extensive attempts to assign them, only weak amide correlations for residues Arg-159 through Val-161 could be identified. Because these residues exhibit low temperature factors in the crystal structure and some of their amides are protected from deuterium exchange in solution, it is possible that they adopt a rigid conformation and that their broadening in the NMR spectra is indirectly caused by flap motions of regions 2 and 3. A similar, but less pronounced broadening is observed in residues in strand $\beta8$, consistent with their more distal positioning underneath the flap. Because broadening is observed in both the presence and absence of Ca^{2+}, the flap must constantly be in motion, presumably sampling the open and closed states prior to binding the sorting signal. Interestingly, the broadened resonances reappear in the NMR spectra of Ca^{2+}-bound SrtA complexed with a peptidyl-sulfhydryl compound that mimics the substrate (data not shown). Although the NMR sample of this complex is too dilute for detailed relaxation studies, the observation of a single set of NMR resonances strongly suggests that the substrate induces the loop to adopt a single conformation.

The precise mode of substrate recognition cannot be gleaned from the recently determined crystal structure of the $^{C184A}SrtA_{\Delta N59}$-LPETG peptide complex because of the high temperature factors of the bound substrate, which indicate that it is structurally disordered. However, the $\beta6/\beta7$ loop in the structure of the complex adopts a conformation more reminiscent of the closed state, which enables the side chains of Val-168 and Leu-169 to bracket the proline ring of the substrate. Because a generally similar conformation is observed in the NMR structure of the Ca^{2+}-bound apo-substrate enzyme, the available data suggest that Ca^{2+} bound to the $\beta3/\beta4$ pocket promotes substrate binding by stabilizing a loop conformation better suited for binding by forming interactions with Glu-171 that help to tether the flap to the protein body.

The increased enzymatic activity of SrtA in response to Ca^{2+} enhances the chances of *S. aureus* colonizing its host by up-regulating the number of proteins it displays on its surface. In other Ca^{2+}-regulated proteins, Ca^{2+} elicits its effects at a structural level, for example, facilitating the correct assembly of enzyme active sites or exposing protein surfaces required for function (57–60). It can also act directly in catalysis by interacting with the substrate or by stabilizing key reaction intermediates through electrostatic effects (61). Here we have shown that, in SrtA, Ca^{2+} promotes substrate binding by modulating both the structure and dynamics of a large substrate-contacting loop. Although

more complex models of motion are possible, the available structural and dynamics data are consistent with a model in which a portion of the loop is generally disordered and capable of toggling between two states (Fig. 6), a binding competent closed form, and a highly flexible open state that removes key substrate contacting residues from the active site. We propose that these conformers are in dynamic equilibrium and that a single Ca^{2+} ion acts to bias the loop toward its binding competent closed form by transiently tethering the C-terminal end of the loop to the body of the protein by contacting the side chain of Glu-171. In other enzymes the dynamic behavior of active site loops has been shown to be important for catalysis (62–64). Interestingly, in SrtA, the magnitude and time scales of these motions are responsive to Ca^{2+}, which when bound allosterically, triggers slow micro- to millisecond motions that may be ideally suited for substrate recognition. Bacteria becoming increasingly resistant to multiple antibiotics is an increasing health concern. The central role of sortases in bacterial virulence makes them an attractive target for new anti-infective agents, and an understanding of how Ca^{2+} regulates their activity should aid in the ongoing development of small molecule inhibitors of this enzyme class (65–67).

Acknowledgments—We thank Drs. Martin Phillips and Robert Peterson for technical assistance. We also thank Professor Arthur Palmer for making the programs used in the relaxation data analysis available.

REFERENCES

1. Connolly, K. M., and Clubb, R. T. (2005) in *Structural Biology of Bacterial Pathogenesis* (Waksman, G., Caparon, M., and Hultgren, C., eds) pp. 101–127, ASM Press, Washington, D. C.
2. Ton-That, H., Marraffini, L. A., and Schneewind, O. (2004) *Biochim. Biophys. Acta* **1694,** 269–278
3. Paterson, G. K., and Mitchell, T. J. (2004) *Trends Microbiol.* **12,** 89–95
4. Mazmanian, S. K., Liu, G., Hung, T. T., and Schneewind, O. (1999) *Science* **285,** 760–763
5. Schneewind, O., Model, P., and Fischetti, V. A. (1992) *Cell* **70,** 267–281
6. Schneewind, O., Mihaylovapetkov, D., and Model, P. (1993) *EMBO J.* **12,** 4803–4811
7. Navarre, W. W., and Schneewind, O. (1994) *Mol. Microbiol.* **14,** 115–121
8. Ruzin, A., Severin, A., Ritacco, F., Tabei, K., Singh, G., Bradford, P. A., Siegel, M. M., Projan, S. J., and Shlaes, D. M. (2002) *J. Bacteriol.* **184,** 2141–2147
9. Perry, A. M., Ton-That, H., Mazmanian, S. K., and Schneewind, O. (2002) *J. Biol. Chem.* **277,** 16241–16248
10. Pallen, M. J., Lam, A. C., Antonio, M., and Dunbar, K. (2001) *Trends Microbiol.* **9,** 97–101
11. Comfort, D., and Clubb, R. T. (2004) *Infect. Immunol.* **72,** 2710–2722
12. Mazmanian, S. K., Liu, G., Jensen, E. R., Lenoy, E., and Schneewind, O. (2000) *Proc. Natl. Acad. Sci. U. S. A.* **97,** 5510–5515
13. Bolken, T. C., Franke, C. A., Jones, K. F., Zeller, G. O., Jones, C. H., Dutton, E. K., and Hruby, D. E. (2001) *Infect. Immun.* **69,** 75–80
14. Bierne, H., Mazmanian, S. K., Trost, M., Pucciarelli, M. G., Liu, G., Dehoux, P., Jansch, L., Garcia-del Portillo, F., Schneewind, O., and Cossart, P. (2002) *Mol. Microbiol.* **43,** 869–881
15. Garandeau, C., Reglier-Poupet, H., Dubail, L., Beretti, J. L., Berche, P., and Charbit, A. (2002) *Infect. Immun.* **70,** 1382–1390
16. Jonsson, I. M., Mazmanian, S. K., Schneewind, O., Verdrengh, M., Bremell, T., and Tarkowski, A. (2002) *J. Infectious Dis.* **185,** 1417–1424
17. Ilangovan, U., Ton-That, H., Iwahara, J., Schneewind, O., and Clubb, R. T. (2001) *Proc. Natl. Acad. Sci. U. S. A.* **98,** 6056–6061
18. Zong, Y., Bice, T. W., Ton-That, H., Schneewind, O., and Narayana, S. V. (2004) *J. Biol. Chem.* **279,** 31383–31389
19. Ton-That, H., Liu, G., Mazmanian, S. K., Faull, K. F., and Schneewind, O. (1999) *Proc. Natl. Acad. Sci. U. S. A.* **96,** 12424–12429
20. Ton-That, H., Mazmanian, S. K., Alksne, L., and Schneewind, O. (2002) *J. Biol. Chem.* **277,** 7447–7452
21. Marraffini, L. A., Ton-That, H., Zong, Y., Narayana, S. V., and Schneewind, O. (2004) *J. Biol. Chem.* **279,** 37763–37770
22. Liew, C. K., Smith, B. T., Pilpa, R., Suree, N., Ilangovan, U., Connolly, K. M., Jung, M. E., and Clubb, R. T. (2004) *FEBS Lett.* **571,** 221–226
23. Connolly, K. M., Smith, B. T., Pilpa, R., Ilangovan, U., Jung, M. E., and Clubb, R. T. (2003) *J. Biol. Chem.* **278,** 34061–34065
24. Mao, H., Hart, S. A., Schink, A., and Pollok, B. A. (2004) *J. Am. Chem. Soc.* **126,** 2670–2671
25. Huang, X., Aulabaugh, A., Ding, W., Kapoor, B., Alksne, L., Tabei, K., and Ellestad, G. (2003) *Biochemistry* **42,** 11307–11315
26. Kay, L. E., Keifer, P., and Saarinen, T. (1992) *J. Am. Chem. Soc.* **114,** 10663–10665
27. Kordel, J., Skelton, N. J., Akke, M., Palmer, A. G., 3rd, and Chazin, W. J. (1992) *Biochemistry* **31,** 4856–4866
28. Skelton, N. J., Palmer, A. G., 3rd, Akke, M., Kordel, J., Rance, M., and Chazin, W. J. (1993) *J. Magn. Reson.* **102,** 253–264
29. Delaglio, F. (1995) *J. Biomol. NMR* **6,** 277–293
30. Goddard, T. D., and Kneller, D. G. (2001) *Sparky 3 NMR Software*, University of California, San Francisco
31. Tjandra, N., Kuboniwa, H., Ren, H., and Bax, A. (1995) *Eur. J. Biochem.* **230,** 1014–1024
32. Kneller, J. M., Lu, M., and Bracken, C. (2002) *J. Am. Chem. Soc.* **124,** 1852–1853
33. Koradi, R., Billeter, M., and Wuthrich, K. (1996) *J. Mol. Graphics* **14,** 51–55
34. Garcia de la Torre, J., Huertas, M. L., and Carrasco, B. (2000) *J. Magn. Reson.* **147,** 138–146
35. Farrow, N. A., Muhandiram, R., Singer, A. U., Pascal, S. M., Kay, C. M., Gish, G., Shoelson, S. E., Pawson, T., Forman-Kay, J. D., and Kay, L. E. (1994) *Biochemistry* **33,** 5984–6003
36. Lee, L. K., Rance, M., Chazin, W. J., and Palmer, A. G., 3rd. (1997) *J. Biomol. NMR* **9,** 287–298
37. Bruschweiler, R. (2003) *Curr. Opin. Struct. Biol.* **13,** 175–183
38. Bruschweiler, R., Liao, X., and Wright, P. E. (1995) *Science* **268,** 886–889
39. Lipari, G., and Szabo, A. (1982) *J. Am. Chem. Soc.* **104,** 4546–4559
40. Lipari, G., and Szabo, A. (1982) *J. Am. Chem. Soc.* **104,** 4559–4570
41. Mandel, A. M., Akke, M., and Palmer, A. G., 3rd. (1996) *Biochemistry* **35,** 16009–16023
42. Mandel, A. M., Akke, M., and Palmer, A. G., 3rd. (1995) *J. Mol. Biol.* **246,** 144–163
43. Hu, W., Lee, K. C., and Cross, T. A. (1993) *Biochemistry* **32,** 7035–7047
44. Korzhnev, D. M., Salvatella, X., Vendruscolo, M., Di Nardo, A. A., Davidson, A. R., Dobson, C. M., and Kay, L. E. (2004) *Nature* **430,** 586–590
45. Mueller, G. A., Pari, K., DeRose, E. F., Kirby, T. W., and London, R. E. (2004) *Biochemistry* **43,** 9332–9342
46. Ubach, J., Zhang, X., Shao, X., Sudhof, T. C., and Rizo, J. (1998) *EMBO J.* **17,** 3921–3930
47. Rizo, J., Ubach, J., and Garcia, J. (2002) *Methods Mol. Biol.* **172,** 305–316
48. Vogel, H. (2002) in *Calcium-binding Protein Protocols: Reviews and Case Studies* (Vogel, H., ed) Vol. 1, pp. 3–20, 2 vols., Humana Press, Totowa, NJ
49. Hu, H., Sheehan, J. H., and Chazin, W. J. (2004) *J. Biol. Chem.* **279,** 50895–50903
50. Kruger, R. G., Otvos, B., Frankel, B. A., Bentley, M., Dostal, P., and McCafferty, D. G. (2004) *Biochemistry* **43,** 1541–1551
51. Volkman, B. F., Lipson, D., Wemmer, D. E., and Kern, D. (2001) *Science* **291,** 2429–2433
52. Eisenmesser, E. Z., Bosco, D. A., Akke, M., and Kern, D. (2002) *Science* **295,** 1520–1523
53. Loria, J. P., Rance, M., and Palmer, A. G., 3rd. (1999) *J. Am. Chem. Soc.* **121,** 2331–2332
54. Palmer, A. G., 3rd, Kroenke, C. D., and Loria, J. P. (2001) *Methods Enzymol.* **339,** 204–238
55. Ishima, R., and Torchia, D. A. (1999) *J. Biomol. NMR* **14,** 369–372
56. Millet, O., Bernado, P., Garcia, J., Rizo, J., and Pons, M. (2002) *FEBS Lett.* **516,** 93–96
57. Finn, B. E., Evenas, J., Drakenberg, T., Waltho, J. P., Thulin, E., and Forsen, S. (1995) *Nat. Struct. Biol.* **2,** 777–783
58. Moldoveanu, T., Hosfield, C. M., Lim, D., Elce, J. S., Jia, Z., and Davies, P. L. (2002) *Cell* **108,** 649–660
59. Kuboniwa, H., Tjandra, N., Grzesiek, S., Ren, H., Klee, C. B., and Bax, A. (1995) *Nat. Struct. Biol.* **2,** 768–776
60. Zhang, M., Tanaka, T., and Ikura, M. (1995) *Nat. Struct. Biol.* **2,** 758–767
61. Steegborn, C., Litvin, T. N., Levin, L. R., Buck, J., and Wu, H. (2005) *Nat. Struct. Mol. Biol.* **12,** 32–37
62. Rozovsky, S., and McDermott, A. E. (2001) *J. Mol. Biol.* **310,** 259–270
63. Wang, L., Pang, Y., Holder, T., Brender, J. R., Kurochkin, A. V., and Zuiderweg, E. R. (2001) *Proc. Natl. Acad. Sci. U. S. A.* **98,** 7684–7689
64. McElheny, D., Schnell, J. R., Lansing, J. C., Dyson, H. J., and Wright, P. E. (2005) *Proc. Natl. Acad. Sci. U. S. A.* **102,** 5032–5037
65. Oh, K. B., Kim, S. H., Lee, J., Cho, W. J., Lee, T., and Kim, S. (2004) *J. Med. Chem.* **47,** 2418–2421
66. Frankel, B. A., Bentley, M., Kruger, R. G., and McCafferty, D. G. (2004) *J. Am. Chem. Soc.* **126,** 3404–3405
67. Scott, C. J., McDowell, A., Martin, S. L., Lynas, J. F., Vandenbroeck, K., and Walker, B. (2002) *Biochem. J.* **366,** 953–958
68. Andre, I., and Linse, S. (2002) *Anal. Biochem.* **305,** 195–205